IJMCM 13 (2) (2023) 1889-1905 Doi: 10.22034/IJMCM.2023.708106

International Journal of
Molecular and Clinical Microbiology

Research Article

Antimicrobial and Cytotoxic Effects of Synthesized Ag-doped ZnO Nanoparticles on *Listeria monocytogenes* Isolated from Traditional Cheese Using Caco-2 Cell Line

Mojgan Dalirsaber Jalali[1], Khosro Issazadeh[1]*, Ali Abdolahzadeh Ziabari[2], Mirsasan Mirpour[1]

1. Department of microbiology, Lahijan Branch, Islamic Azad Univercity, Lahijan, Iran
2. Nano Research Lab, Lahijan Branch, Islamic Azad Univercity, Lahijan, Iran

ARTICLE INFO

Article history:
Received 8 Jaunuary 2023
Accepted 13 October 2023
Available online 1 November 2023

keywords:
ZnO, ZnO:Ag NPs,
Antibacterial activity,
Listeria monocytogenes,
MTT assay,
Real-time PCR

ABSTRACT

Listeriosis, caused by *Listeria monocytogenes* (*L. monocytogenes*), ranks among the most severe and threatening foodborne diseases. This study investigates the antibacterial, anti-adhesion and anti-invasion effects of Ag-doped ZnO nanoparticles (ZnO:Ag NPs) synthesized against *L. monocytogenes* isolates, focusing on their interaction with Caco-2 cell lines. ZnO and ZnO:Ag NPs were synthesized using a chemical method and characterized through X-ray diffraction (XRD), scanning electron microscopy (SEM), Energy Dispersive X-ray (EDX) analysis and Fourier-transform infrared (FTIR) spectroscopy. The antibacterial activity of the nanoparticles against *L. monocytogenes* was evaluated through culture turbidity measurements. In addition to antibacterial assessments, we employed Caco-2 cell lines to explore the anti-adhesive and anti-invasive properties of these nanoparticles. Specifically, the attachment of *L. monocytogenes* isolates to Caco-2 cells was significantly reduced after treatment with sub-MIC of ZnO:Ag NPs, with the LM4 isolate showing the most pronounced attachment to Caco-2 cell surfaces. Furthermore, invasion assays were conducted to test the ability of *L. monocytogenes* isolates to invade Caco-2 cells before and after treatment with sub-MIC of ZnO:Ag nanoparticles. Prior to treatment, all isolates exhibited high invasion efficiencies (more than 6 Log10 CFU/mL) during a 24-hour period. However, exposure to the nanoparticles resulted in lower bacterial counts (approximately 5 Log10 CFU/mL) over the same duration. Real-time PCR (RT-PCR) analysis confirmed a substantial downregulation of mRNA levels of invasion and adhesion-associated genes (*inlA*, *hlyA* and *prfA*) in *L. monocytogenes* following exposure to ZnO:Ag NPs, compared to the 16S rRNA housekeeping gene. These findings highlight the potential of ZnO:Ag NPs as versatile agents in medical and pharmaceutical applications, owing to their significant antibacterial, anti-adhesive and anti-invasive properties, particularly when interacting with Caco-2 cell lines.

1. Introduction

Listeria monocytogenes (*L. monocytogenes*) is a facultative intracellular pathogen, a non-spore-forming, aerobic, gram-positive bacillus and the causative agent of listeriosis in both humans and animals. It represents a significant source of microbial contamination, particularly

*Corresponding authors: Khosro Issazadeh
Email address: issa_kaam@yahoo.com

on industrial surfaces, posing a substantial threat to the food chain (Abdellrazeq et al., 2014; Ayaz et al., 2018). *L. monocytogenes* infection is associated with a fatality rate of 15%-20% and is a major cause of abortion in pregnant women, as well as encephalitis, meningitis and septicemia in newborn infants and immunocompromised patients (Bayda et al., 2019). Additionally, *L. monocytogenes* can develop resistance to certain antimicrobials, especially cephalosporins. Furthermore, it can modulate various genes that induce β-lactam production and confer resistance to certain β-lactams and lantibiotics (Brandt et al., 2012). Innovative approaches, including the use of bacteriophages and bacteriocins, have been explored to mitigate the incidence of *L. monocytogenes* in food processing environments. This not only reduces the risk of food contamination but also contributes to public health risk reduction (Burlibaşa et al., 2020).

L. monocytogenes is well-adapted to surviving in both soil and eukaryotic host cell cytosols and can contribute to human infections as an intracellular pathogen (Cardoza-Contreras et al., 2019). The virulence of *L. monocytogenes* relies on its ability to adhere to and invade host cell surfaces, replicate intracellularly and spread from cell to cell (Carvalho et., 2014). Each of these stages is contingent upon specific virulence factors that disrupt host cell functions (Dakal et al., 2016). Numerous virulence genes associated with the *L. monocytogenes* infection process have been identified and their pathogenic effects have been well elucidated. Six primary virulence genes, located in the Listeria Pathogenicity Island (*prfA*, *plcA*, *hly*, *mpl*, *actA* and *plcB*), are involved in bacterial adhesion and invasion of host cells (Dussurget et al., 2002; Fahmy et al., 2019). In this study, we assessed the expression of three genes *hlyA*, *inlA* and *prfA* as target markers to characterize the pathogenicity of *L. monocytogenes* isolates.

The listerial internalin (InlA) protein plays a crucial role in mediating invasion of epithelial cells and bacterial adhesion. Transcription of the encoding gene can occur through both PrfA-independent and PrfA-dependent mechanisms (Fonseca et al., 2019). E-cadherin has been identified as the receptor for InlA, allowing it to enter epithelial cells on the luminal surface of intestinal villi, cytotrophoblasts, and areas of syncytiotrophoblasts. Several reports have indicated the overexpression of the *inlA* gene in isolates from human cases of listeriosis, underscoring the pivotal role of *inlA* in the disease process (Fontecha-Umaña et al., 2020). Following bacterial entry into host cells and phagocytosis, listeriolysin O, encoded by the *hlyA* gene, is responsible for lysing and escaping from the phagocytic vacuole. This enables bacterial propulsion into the host cytosol and replication (Gray et al., 2018). Subsequently, *L. monocytogenes* can express the *prfA* gene, which is essential for the activation of the *inlAB* operon (Ghosh et al., 2015).

Nanotechnology is a field of science that involves manipulating individual atoms and molecules to create novel materials with exceptionally diverse properties and numerous applications (Hasan et al., 2018). Nanoparticles possess unique physical and chemical properties categorized based on size, chemical ractivity, energy absorption and biological mobility. This technology has been applied in various fields through an integrated approach (Hosu et al., 2019). Nanomedicine represents a significant advancement in the medical field, utilizing nanomaterials for various applications such as disease diagnosis, monitoring, control, prevention and treatment. Its capabilities encompass protein detection, DNA structure probing, tissue engineering, hyperthermia-based tumor destruction, biological molecule and cell separation and purification, enhanced MRI contrast, phagokinetic studies, drug and gene delivery and acting as agents for combatting cancer, microbial infections, fungal diseases, as well as serving as fluorescent biological labels (Jamshidi and Zeinali, 2019; Kołodziejczak-Radzimska, Jesionowski, 2014).

Zinc oxide (ZnO) nanocrystals are biocompatible materials that can be doped with silver (Ag) or silver oxide (Lemon et al., 2010) nanocrystals (Li et al. 2018). ZnO nanocrystals possess significant features such as high catalytic activity, chemical and physical stability and ultraviolet absorption (Abdellrazeq et al., 2014). ZnO also finds extensive use, particularly in environmental photocatalytic degradation of pollutants (Li et al., 2018). Despite their promising properties, ZnO nanoparticles present certain limitations for research, including poor dispersion, aggregation and a wide energy gap (Miri et al., 2019). Doping proves to be an effective technique for enhancing catalytic

activity in ZnO nanocrystals and addressing these challenges. It can induce oxidative stress in various bacteria, promoting the generation of reactive oxygen species (ROS), thereby elucidating the bactericidal action of Ag-doped ZnO nanocrystals (Miri et al., 2019; Mirzaei and Darroudi, 2017). Both ZnO and Ag nanoparticles have been widely applied in numerous critical fields owing to their advantageous nanoscale physical characteristics (Mohammadi et al., 2018; Moulavi et al., 2019). Extensive data indicate that metal ion-doped ZnO nanostructures, especially Ag-doped ZnO, exhibit potent photocatalytic and antimicrobial properties, along with toxicity against a broad range of bacteria (Nguyen and Portnoy, 2020). Therefore, this study aimed to investigate the synergistic toxic effects of nanocomposites composed of Ag-doped ZnO on controlling and preventing the proliferation of *L. monocytogenes*. Additionally, we aimed to confirm the internalization of *L. monocytogenes* into mammalian cultured cells, with a primary focus on three internalization factors: *inlA*, *hlyA* and *prfA*.

2. Materials and Methods

2.1. Synthesis of Ag-doped ZnO NPs

For the synthesis of undoped and Ag-doped ZnO nanostructures, high purity zinc nitrate ($Zn(NO_3)_2$), silver nitrate ($AgNO_3$) and sodium hydroxide (NaOH) solution were used as the precursor and isopropanol ($(CH_3)_2CHOH$) was applied as the solvent. In a typical procedure for the synthesis of pure ZnO NPs, 0.05 M zinc nitrate and 0.1 M NaOH solution were dissolved in 100 ml of propanol, then 250 ml NaOH solution was added dropwise to zinc nitrate solution, until the pH became 12. When Sodium hydroxide solution is added a white precipitate is formed which is soluble in excess of sodium hydroxide. Similarly for the synthesis of Ag-doped ZnO NPs, 0.5 M concentration of AgNO3 was added to the 0.1 M zinc nitrate solution and NaOH solution and then, the Ag-doped ZnO NPs were obtained from the $Ag(OH)_2$ precipitate. The nanohybrids were collected by centrifugation at high speed (10,000 rpm) for 5 min. The residual precursors and agents were then fully removed after several rounds of centrifugation by adding fresh distilled water. Finally, It was dried in oven at 100°C for 2 hrs (Ghosh et al., 2015).

2.2. Characterization

XRD-6000 X-Ray Diffractometer (Shimadzu, Japan) with CuKα radiation (λ = 0.15406 nm) was used for the crystal phase analysis of the both doped and undoped NPs powders. Fourier-transform infrared spectroscopy (FTIR) were applied to identify the functional agents and recorded over a wavenumber range of 400–4000 cm^{-1} with a 4 cm^{-1} resolution and ordinate (Shidmuzu, Japan). The particle size, morphology and surface composition were analyzed using a scanning electron microscope (SEM) equipped with energy-dispersive X-ray spectroscopy (EDS) (CM120, Philips, Netherlands).

2.3. Selection and preparation of Listeria monocytogenes

In this study, we collected 200 traditional fresh cheese samples from various geographical locations in Gilan province, including Lahijan and Rasht cities. We isolated three *L. monocytogenes* strains (3%) from these samples using the cold enrichment method. Briefly, 25g of each cheese sample was aseptically added to 225ml of Listeria Enrichment broth and homogenized using a Stomacher. The homogenized samples were incubated at 4°C for one week. After incubation, we streaked the samples onto 5% Listeria enrichment agar. Colonies displaying morphology typical of Listeria spp. were further purified on Brain Heart Infusion (BHI) agar medium and confirmed using different species-specific tests. The characterization process involved Gram staining, motility and Catalase tests, assessment of hemolysis characteristics, carbohydrate utilization assays and CAMP (Christie–Atkins–Munch–Peterson) tests. These standard methods were in accordance with the guidelines outlined in the USFDA/CFSAN Bacteriological Analytical Manual. Additionally, working stocks of the isolates by sub-culturing them on BHI agar plates and subsequently storing them at -80°C in BHI broth containing 15% glycerol for long-term storage.

2.4. Determination of Antibacterial Activity

Antibacterial activity of ZnO and ZnO:Ag nanoparticles was determined against *L. monocytogenes* isolates from traditional cheese and *L. monocytogenes* PTCC1168 following a slightly modified broth microdilution method outlined by CLSI (Jeevanandam, Barhoum, Chan et al. 2018). The bacterial strains were routinely cultivated on 20 ml of Mueller-Hinton agar (MHB, Merck Germany) and the bacterial cultures were routinely incubated at 37°C. Turbidity was adjusted to 0.5 McFarland standards (1.5×10^8 CFU/mL) by measuring absorbance at 625 nm using a spectrophotometer. Stable colloidal suspensions of ZnO and ZnO:Ag nanostructured with different concentrations (3.125, 6.25, 12.5, 25, 50 and 100 µg/ml) was added to each well. The minimum inhibitory concentration (MIC) was recorded as the lowest concentration that produced a complete inhibition of visible growth in the microtitre plate. The minimum bactericidal concentration (MBC) of the nanoparticles was announced as the lowest concentration totally preventing bacterial growth after incubation at 37°C for 24 h. *L. monocytogenes* PTCC1168 was used as control bacteria. All experiments were performed in triplicate and all data were expressed as the mean. ± standard deviation.

2.5. Detection Inhibitory Activity

For recognizing the inhibitory activity of ZnO:Ag NPs on *L. monocytogenes*, the Tryptic Soy Broth culture, (TSB; Merck, Germany), which contained sub-MIC of NPs, was inoculated with 10^7 cells/ml of *L. monocytogenes*. The bottles were shaken at 50 rpm and kept at a temperature of 37°C. Then, bacterial growth was serially monitored by absorbance at 600 nm in 24, 48 and 72 h. The cultured strains were used as the control without any NP formulation and under the same growth conditions (Ghosh, Das, Jena et al. 2015).

2.6. MTT assay

Caco-2 cell line (caucasian colon adenocarcinoma cells) was purchased from Pasteur institute of Iran (cell bank), Tehran, Iran. The cells were cultured in RPMI 1640 (Gibco, UK) supplemented with 10% heat inactivated fetal bovine serum (Gibco, UK), 100 units/mL penicillin and 100 µg /ml streptomycin and incubated at 37°C in 5% CO2 incubator for 48 hrs.

The MTT [3-(4,5-dimethylthiazol-2-yl)-2,5-diphenyltetrazolium bromide] assay was performed for assessing cell proliferation activity and cytotoxicity in Caco-2 cells exposed to *L. monocytogenes* treated with 3.125, 6.25, 12.5, 25, 50 and 100 µg /ml concentrations of both ZnO and ZnO:Ag NPs. Cell viability was determined using the MTT assay 24 hours after incubation. The MTT assays were performed according to standard protocols (Kobayashi et al., 2013; Ahmadian et al., 2009). The cells were seeded in 96-well plates with 1×10^4cells/well and placed at 37°C in a 5% CO2 humidified incubator until 60% confluency. The complete growth medium was removed and the cells were serum-starved for 24 h prior to treatment. Cells incubated in culture medium alone served as a control for cell viability (untreated cells). The cells were exposed to *L. monocytogenes* treated with 3.125, 6.25, 12.5, 25, 50 and 100 µg /ml concentrations of both ZnO and ZnO:Ag NPs for 24 h in complete growth medium. Following the *L. monocytogenes* exposure, the medium was removed and 100 µl of MTT solution (5 mg/mL in sterile H2O) was added to each well. The plates were incubated under 95% atmosphere air and 5% CO2 at 37°C for 4 h. The MTT solution was removed and 200 µl aliquots of DMSO were added to each well to dissolve the formazan crystals followed by incubation for 10 min at 37°C. Treatments were performed in triplicates and optical densities were read at 570 nm by spectrophotometric method.

2.7. Adhesion and invasion assays

The adhesion and invasion assays were performed by infecting semiconfluent Caco-2 cell monolayers grown in 24-well plates. Bacterial cultures containing logarithmically grown bacteria (MOI: 100 bacteria/cell) and ZnO and ZnO:Ag NPs at different concentrations were incubated with cells for 1 hr at 37°C. After this incubation period, cells were extensively washed, lysed with ice-cold 0.1% Triton X- 100 and plated on TSA to determine bacterial adherence. Adhesion afficiency was

expressed as the percent of the inoculated CFU that were recovered. The percentage of bacterial adhesion to Caco-2 cells in presence of NPs was evaluated respect to the percentage of adhesion of *L. monocytogenes* in absence of NPs, considered as 100%.

For invasion assays, after washing, 1 ml of fresh medium containing 50 mg/ml of gentamicin was added to each well and maintained for 1 h at 37°C. Cells were then lysed as for adhesion assay. Invasion efficiency was expressed as the percent of inoculated bacteria that were recovered. The percentage of invasion of bacteria to Caco-2 cells in presence of NPs was evaluated respect to the percentage of invasion of listeria in absence of NPs, considered as 100%.

2.8. Evaluation of inlA, hlyA and prfA genes expression by Real-time PCR

L. monocytogenes isolates was inoculated on TSB medium containing sub-MIC concentration of the both ZnO and ZnO:Ag NPs and then incubated at 37°C overnight. Eventually, the medium was centrifuged at 10,000 g for 20 minutes, the supernatant was disposed and RNA was extracted using RNX-Plus kit (SinaColon Co) according to the manufacturer's instructions. The bacterial suspension without NPs served as control. The ratio of the absorbance at 260 and 280 nm (A260/280) was used to assess the purity and concentration of RNA via a spectrophoto-meter. RNA quality also was assessed by 1.2% agarose gel electrophoresis for 1 h at 100 V. cDNA synthesis was performed using Revert Aid First Strand cDNA Synthesis Kit (Thermo Fisher Scientific) by RT-PCR method on two µg of the treated RNA, according to the manufacturer's company. The primer sets were designed for each gene with Oligo7 software (Table 1).

Real-time quantitative PCR was carried out in a 25µl reaction volume containing 5µl of the appropriate cDNA, 12.5 µl of SYBR Green PCR master mix (Applied Biosystems) and a 600 nM concentration of the appropriate genes specific primers using the ABI STEPONE (Applied Biosystems StepOne™). PCR amplification were performed under the following cycle profile: 95°C followed by one cycle 10 min, 95°C followed by 40 cycle of 15 seconds and 54°C for 1 min. A melting-curve analysis between 55°C and 95°C was conducted after each PCR to verify the amplification product. In current study, the $2^{-\Delta\Delta CT}$ method was applied to analyze the relative changes in gene expression from real-time quantitative PCR experiments. One-way Analysis of Variance (ANOVA) and Tukey's post hoc-test were used to determine significant difference between treatments ($P<0.05$) in SPSS 16 software.

Table 1. Primers for real-time PCR

Primer	Gene type		
	prfA	***hlyA***	***inlA***
Forward	5'-TCATCGACGGCAACCTCGG-'3	5'GAACCAGCTAAGCCIGTAAAAG-'3	5'-CGGAGGTTCCGCAAAAGATG-'3
Reverse	5'-TGAGCAACGTATCCTCCAGAGT-'3	5'-CGCCIGTTTGGGCATCA-'3	5'-CCTCCAGAGTGATCGATGTT-'3

3. Results

3.1. Characterization of prepared ZnO and ZnO:Ag nanoparticles

Figures 1a and 1b show the XRD results of ZnO and ZnO:Ag NPs. Diffraction peaks of ZnO samples had corresponded to hexagonal ZnO with wurtzite structure according to the JCPDS standard card no. 36-1451. Having similar ionic radius Zn^{2+} (0.57 Å) can be replaced in the lattice by Ag^{1+} (0.60 Å). Therefore, substitution of silver has no significant changes in the lattice parameters.

The well-known Scherrer formula was used to evaluate the crystalline size of nanoparticles. Results of calculation showed the average grain size of 27.2 nm for ZnO NPs and 22.4 nm for Ag-doped ZnO NPs. The smaller grain size for Ag-doped NPs can be assigned to the lower ionic radius of Ag^{+1} (5.7 nm) than that of Zn^{2+} (6.0 nm). To investigate the surface structure of the NPs, a typical SEM micrograph related to ZnO:Ag NPs was recorded and shown in Fig. 2.

The SEM apparatus was equipped with EDX analyzer. So, the elemental map plus elemental percentage measurements were provided. Results have been shown in Fig. 2b and c, respectively. The related SEM of the prepared NPs contains mainly the polyhedral shaped objects along with nano-rods. Comparing with the obtained results of XRD, one can conclude that the observed shapes involve nono-crystallites with the size measured by Scherrer formula. Both elemental map and elemental transition peaks confirm the presence of Zn, O and Ag on the surface of the synthesized NPs. FTIR analysis has been done to study the surface chemistry and modes of vibrations of chemical bonds present in all the prepared samples (Fig. 3). The FTIR spectra of the pristine ZnO shows three peaks. The broad peak around 3471 cm-1 can be assigned to the absorbed water in nitrates [S Bandyopadhyay, G K Paul, R Roy, S K Sen and S Sen, Mater. Chem. Phys. 74, 83 (2002)]. The intensity of the peaks increased with adding Ag.

3.2. Antibacterial activity of ZnO and ZnO:Ag NPs

The antibacterial activity of ZnO and ZnO:Ag NPs on *L. monocytogenes* isolates was performed using culture turbidity (0.5 MacFarland standard) as qualitative measure of cell growth (figure 4, 5, 6 and 7). According to figures ZnO:Ag NPs have great antibacterial activities against *L. monocytogenes* isolates from cheese and also the most anti-proliferative effect was belong to *L. monocytogenes* number 5 treated by ZnO:Ag NPs with 25 mm diameters.

Antibacterial assay of the prepared nanoparticles towards *L. monocytogenes* was performed using culture turbidity measurement as qualitative assessment Method for bacterial Growth. According to the results of Table 1, the antimicrobial effects of ZnO:Ag NPs was dramatically higher than ZnO NPs alone on the both standard strains of *L. monocytogenes* PTCC1168 and *L. monocytogenes* strains isolated from local cheese. 100 µg/ml of ZnO:Ag NPs has the highest antibacterial activity on standard strains as well as *L. monocytogenes* strains isolated from cheese (Table 1 and 2).

MIC is the lowest concentration of NPs that inhibits bacterial growth, however, MBC is the lowest concentration that kills bacteria. The both synthesized ZnO and ZnO:Ag NPs showed antibacterial activity against *L. monocytogenes* PTCC1168 strains and *L. monocytogenes* strains isolated from local cheese. However, ZnO:Ag NPs has more inhibitory and killing effects than ZnO NPs alone on both standard and isolation strains.

Figure 8a shows the effect of ZnO:Ag nanoparticle treatment on the growth of *L. monocytogenes* in TSB broth at 37°C for 24,48 and 72 h. Treatments with sub-MIC of ZnO:Ag NP exhibit a significant inhibitory effect on the growth of all samples of *L. monocytogenes* during 24, 48 and 72 h of incubation, compared to the control. Among the samples, LM4 isolate had the highest resistance to sub-MIC concentration of nanoparticle (Figure 8b) and ZnO:Ag NPs could dramatically inhibit the growth of LM6 in 24, 48 and 72 h compared to all samples and control. Also, results demonstrated that ZnO:Ag nanoparticle had less inhibitory effect on all isolates in 48h in comparison with 24 and 72 h.

3.3 MTT Assay

Figure 9 demonstrate viability of *L. monocytogenes* isolates exposed to 3.125, 6.25, 12.5, 25, 50 and 100 µg/ml of both ZnO and ZnO:Ag NPs.

According to figure 9, Caco-2 cells viability significantly decreased in exposed to isolates treated with 25, 50 and 100 µg/ml of both NPs compared to control group ($P<0.001$). There was also significant difference in cells viability treatment with isolates exposed to 12.5 µg/ml of both ZnO and ZnO:Ag NPs ($P<0.05$ and $P<0.001$, respectively). However, isolates treated with 6.25 µg/ml of ZnO:Ag NPs only could dramatically reduce the viability of Caco-2 cells ($P<0.01$) and bacteria isolates which were treated with 6.25 µg/ml of ZnO:Ag NPs, had no effect on viability of Caco-2 cells. There was no significant difference between viability of cells in exposed to isolates treated with 3.125 µg/ml of both NPs compared to control group. Paper results also indicated exposure of *L. monocytogenes* isolates treated with all concentration of ZnO:Ag NPs could obviously reduce the viability of cells compared to control

group and Caco-2 cells exposed to bacteria which were treated with ZnO NPs.

To investigate the effect of synthesized nanoparticles (ZnO and ZnO:Ag NPs) on human cell lines, the cytotoxicity assay was conducted on Caco-2 cell lines. The microtitre plates were examined for morphological changes in cell lines. After incubation with both ZnO and ZnO:Ag NPs, the results were examined at 24 h. According to figure 10, Caco-2 cells started to change morphologically and changes were clearer with the IC50 of both ZnO (46.56 µg/ml) and ZnO:Ag NPs (10.47 µg/ml) at 24 h.

3.4 Attachment and invasion

Figure 11 shows the attachment of *L. monocytogenes* isolates treated with sub-MIC of ZnO:Ag NPs to Caco-2 cell lines. According to results, the attachment of all isolates to Caco-2 cells decreased remarkably compare to control (*L. monocytogenes* strain PTCC 1168), after treatment by ZnO:Ag NPs at sub-MICs. LM4 has been shown the most attachment to Caco-2 cells surfaces between *L. monocytogenes* isolates.

Figure 12 shows *The L. monocytogenes* isolates (LM4, LM5, LM6) were tested for their ability to invade human Caco-2 cells, before and after treatment with sub-MIC of ZnO:Ag nanoparticles.

Results of the invasion assay are presented in Fig. 11 and reported as log10 CFU/mL ± standard deviation.

According to results, all isolates showed high invasion efficiencies (more than 6 (Log10 CFU/mL)) during 24 h, before treatment by sub-MIC of NPs. After exposure of isolates to NPs, all isolates exhibited lower bacterial counts (approximately 5 (Log10 CFU/mL)) during 24 h.

3.5 Relative expression of the virulence genes inlA, hlyA and prfA

The three *L. monocytogenes* strains have been isolated among 100 examined strains. To further confirm the anti-invasion effect of *L. monocytogenes* treated with ZnO:Ag NPs on Caco-2 cell line, the messenger RNA (mRNA) levels of invasion and adhesion-associated genes (*inlA*, *hlyA* and *prfA*) were examined using Real-time PCR. The results of Real-time PCR revealed that the mRNA levels of *inlA*, *hlyA* and *prfA* were dramatically downregulated after the exposure of *L. monocytogenes* treated with ZnO:Ag NPs compared to 16S rRNA as housekeeping gene ($P<0.001$), indicating the anti-invasion and anti-adhesion activity of ZnO:Ag NPs at the transcriptional level (Figure 13).

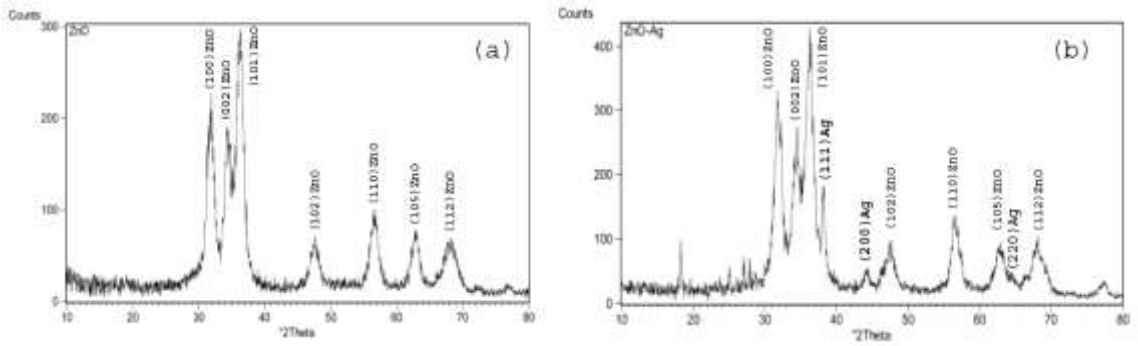

Figure 1. XRD pattern of pure ZnO (a) and ZnO:Ag (b) nanoparticles.

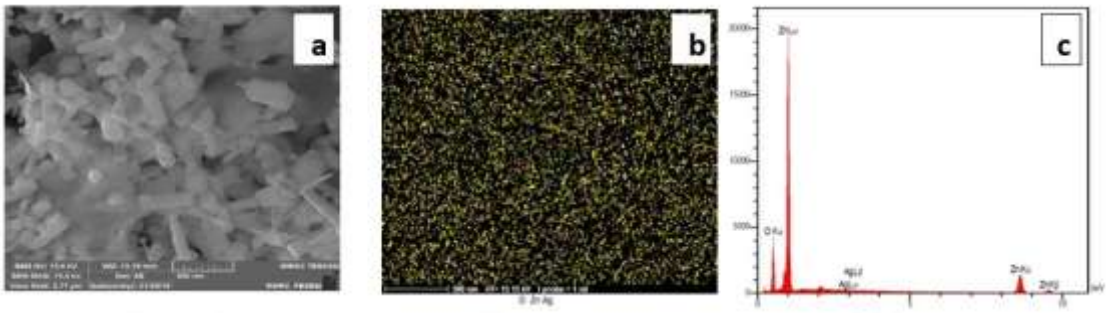

Figure 2. (a) SEM image of ZnO:Ag NPs, (b) ZnO:Ag elemental mapping and (c) EDX spectrum of ZnO:Ag NPs.

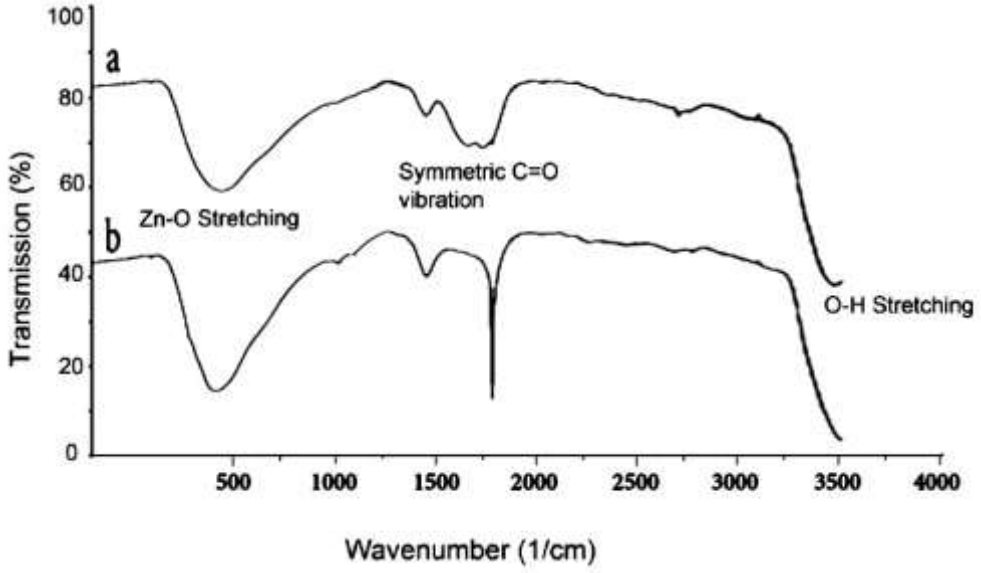

Figure 3. FTIR spectra for (a) ZnO and (b) ZnO:Ag NPs.

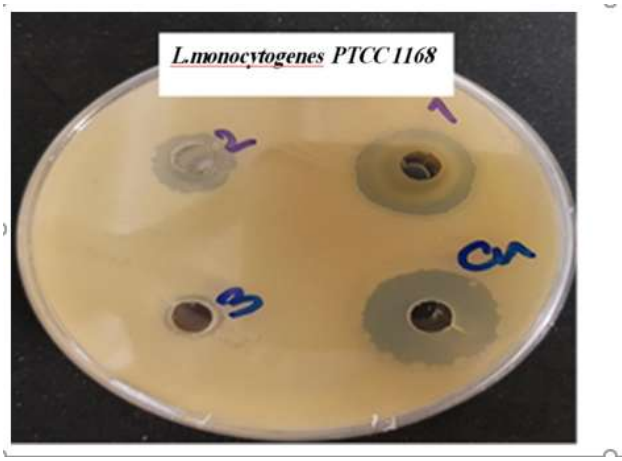

Treatments	Diameter (mm)
ZnO:Ag	22 mm
ZnO	12 mm
Cn-	6 mm
Cn+	28 mm

Figure 4. Antibacterial activity of (1) ZnO:Ag NPs (2) ZnO NPs (3) control negative and (4) antibiotic against *L. monocytogenes* PTCC 1168

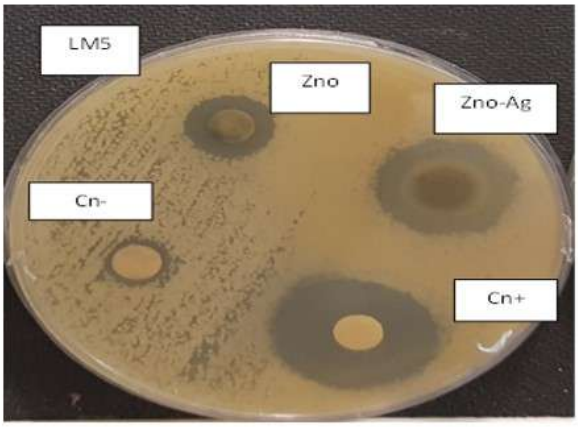

Treatments	Diameter (mm)
Zno	17 mm
Zno-Ag	25 mm
Cn-	6 mm
Cn+	31 mm

Figure 5. Antibacterial activity of ZnO:Ag and ZnO NPs against LM5 compared to control negative and control positive

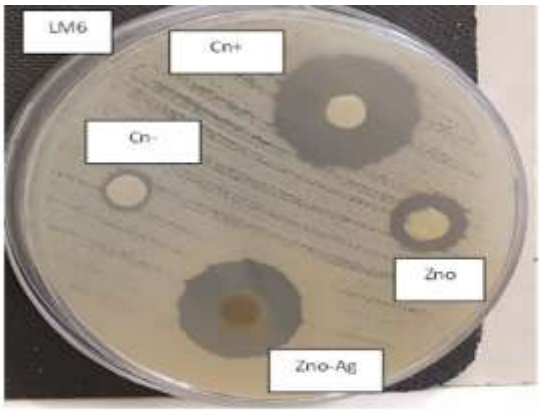

Treatments	Diameter (mm)
Zno	14 mm
Zno-Ag	22 mm
Cn-	6 mm
Cn+	29 mm

Figure 6. Antibacterial activity of ZnO:Ag and ZnO NPs against LM6 compared to control negative and control positive.

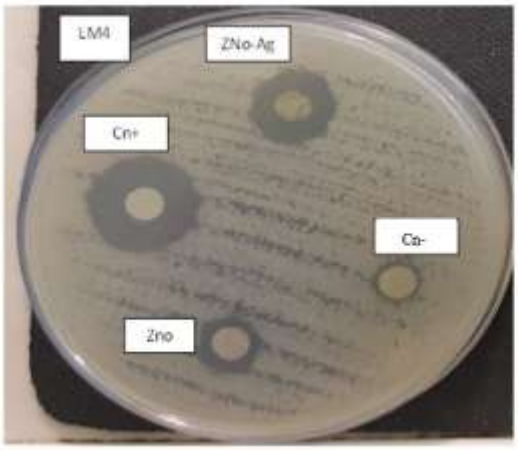

Treatments	Diameter (mm)
Zno	12 mm
Zno-Ag	17 mm
Cn-	6 mm
Cn+	22 mm

Figure 7. Antibacterial activity of ZnO:Ag and ZnO NPs against LM4 compared to control negative and control positive.

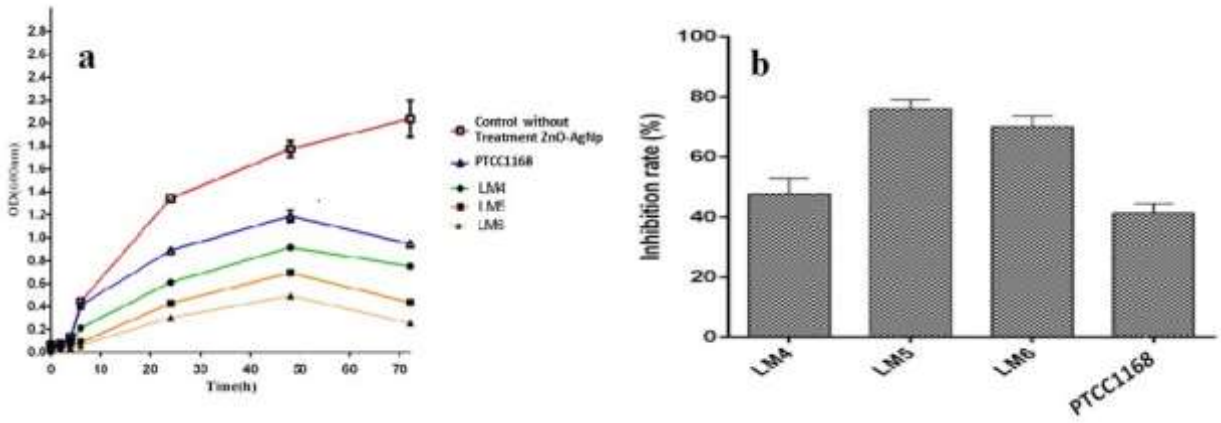

Figure 8. (A) Effect of sub-MIC of ZnO:Ag NP on growth of *L. monocytogenes* isolates and positive and negative controls in TSB at 37 °C during 24, 48 and 72 h. (B) Inhibitory rate of sub-MIC of ZnO:Ag NP on growth of *L. monocytogenes* isolates and positive control.

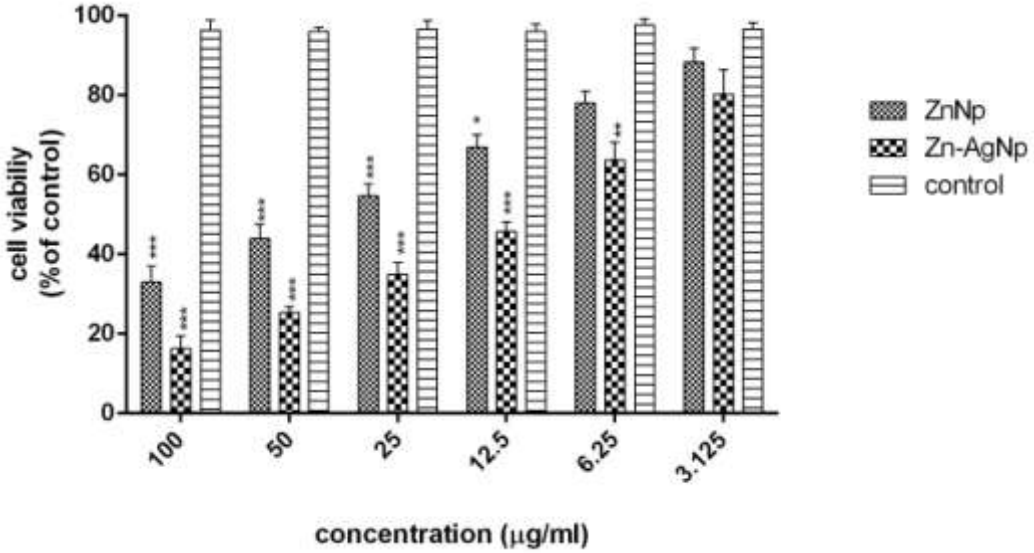

Figure 9. Effect of *L. monocytogenes* isolates treated with different range of concentrations of both ZnO and ZnO:Ag NPs on Caco-2 cells viability. The cells were exposed to isolates which were treated with different concentrations ZnO:Ag NPs (3.125, 6.25, 12.5, 25, 50 and 100 µg/ml). Data are expressed as mean ± SD (n=3) .Values are statistically significant at **P<0.01, *P<0.05 vs. respective control group (One-way ANOVA followed by Tukey's post hoc test).

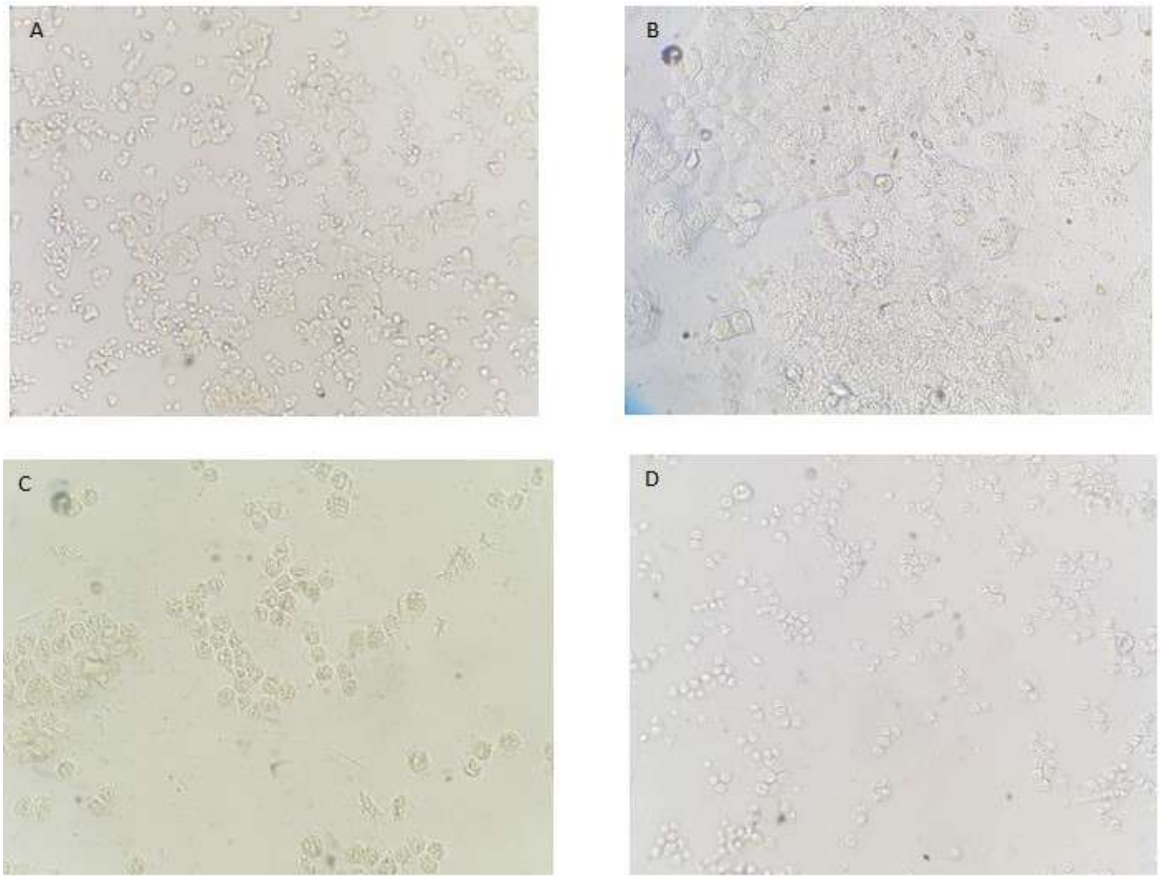

Figure 10. Cytopathic effect of IC50 of ZnO and ZnO:Ag NPs on Caco-2 cells during 24h (100X magnification); (A) Control cells without treatment with NPs (B) Control cells without treatment with NPs after 24h (C) Caco-2 cells treated with IC50 of ZnO NPs after 24h (D) Caco-2 cells treated with IC50 of ZnO:Ag NPs after 24h.

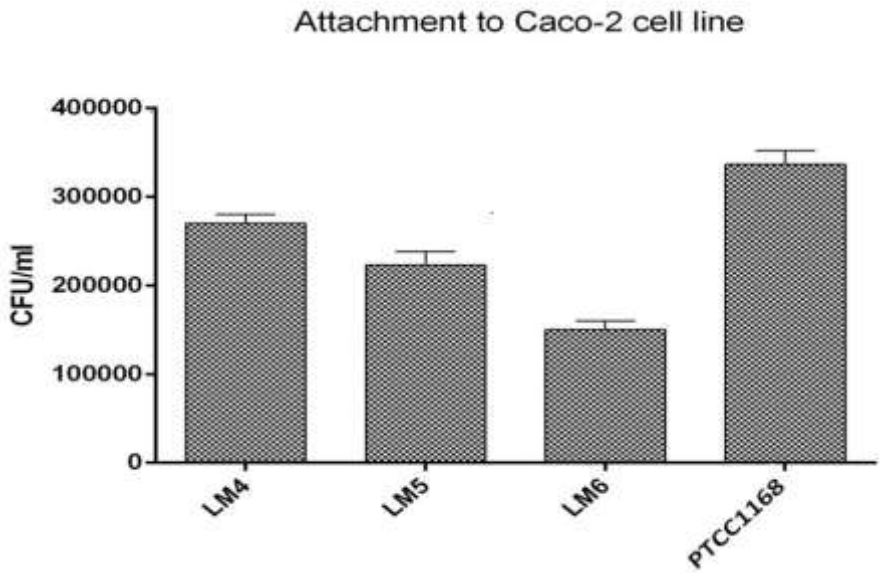

Figure 11. The attachments of *L. monocytogenes* isolates to Caco-2 cells surface.

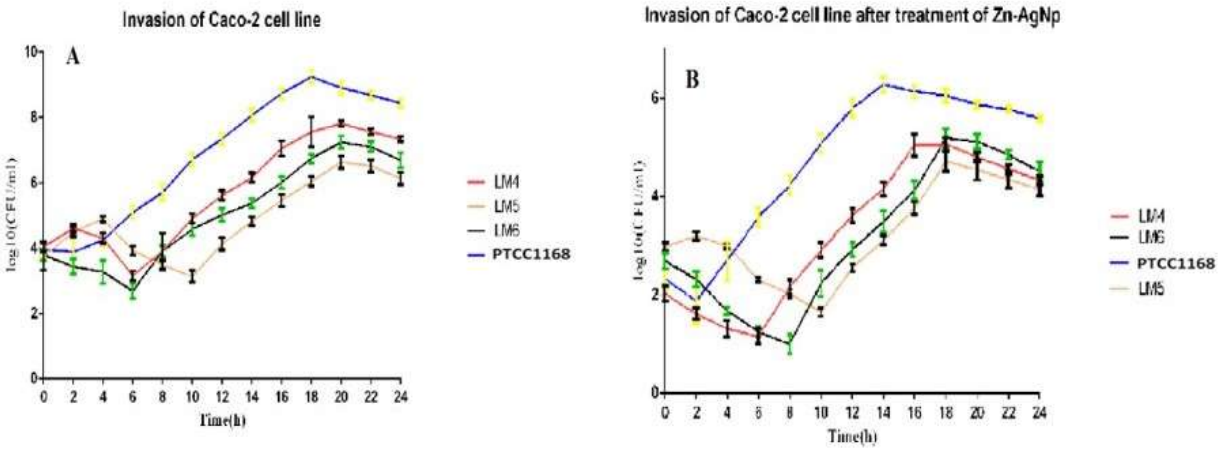

Figure 12. The ability of *L. monocytogenes* isolates to invade human Caco-2 epithelial cells during 24h, before and after treatment with sub-MIC of ZnO:Ag nanoparticles.

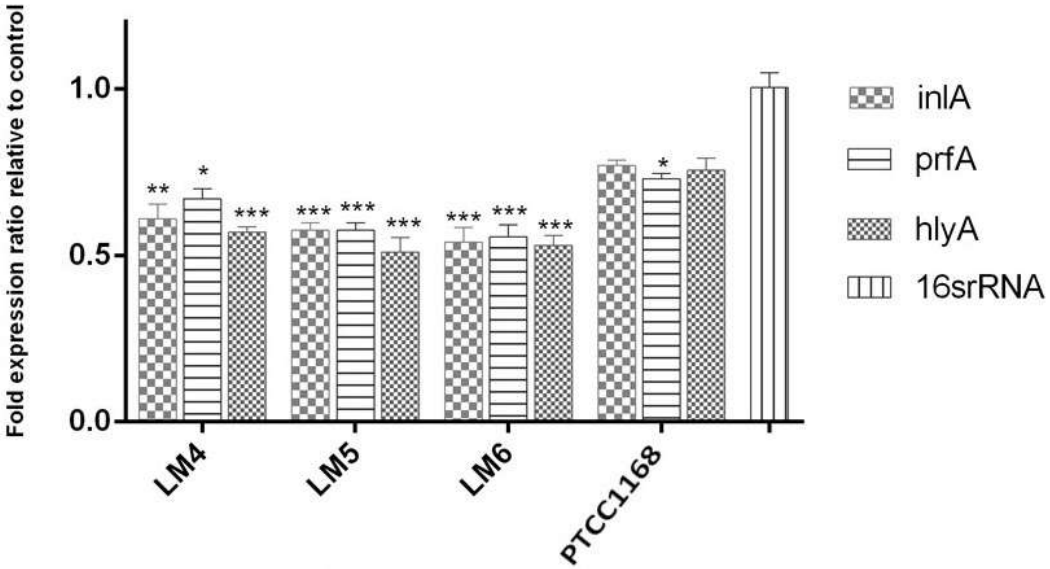

Figure 13. *inlA*, *hlyA* and *prfA* relative gene expression. The relative gene expression for the three *L. monocytogenes* isolates is represented as fold difference between *inlA*, *hlyA*, *prfA* and 16S rRNA gene following treatment with subminimum inhibitory concentration. Data are mean ±standard deviation of three independent experiments. Significant difference specified as ***p < 0.001, **p < 0.01,*p < 0.05.

Table 2. Inhibition zone of *L. monocytogenes* PTCC1168 treated with ZnO and Ag-doped ZnO NPs.

Concentrations (µg/ml)	Inhibition zone (mm)	
	ZnO	Ag-doped ZnO
	Nanoparticles	Nanoparticles
100	11	20
50	10	18
25	9	16
12.5	7	10
6.25	6	9
3.12	6	7

Table 3. Inhibition zone of *L. monocytogenes* isolated from local cheese treated with ZnO and Ag-doped ZnO NPs.

Concentrations(µg /ml)	Inhibition zone(mm)	
	ZnO	Ag-doped ZnO
	Nanoparticles	Nanoparticles
100	7	18
50	7	16
25	6	14
12.5	6	6
6.25	6	6
3.12	6	6

Table 4. Minimum inhibitory concentration (MIC) and minimum bactericidal concentration (MBC) of both ZnO and ZnO:Ag NPs against *L. monocytogenes* PTCC1168 standard strain.

Concentrations(µg /ml)	MIC(mg/ml)	MBC(mg/ml)
ZnO	12.5	25
Ag-doped ZnO	6.25	12.5

Table 5. Minimum inhibitory concentration (MIC) and minimum bactericidal concentration (MBC) of both ZnO and Ag:ZnO NPs against *L. monocytogenes* isolates from cheese.

Concentrations(µg /ml)	MIC(mg/ml)	MBC(mg/ml)
ZnO	50	100
Ag-doped ZnO	12.5	25

4. Discussion

Nanotechnology has found numerous applications in major areas of science, including targeted cancer treatment, novel approaches in biology and the development of unique materials for pathogen detection and treatment (Ortega et al., 2017). For a long time, both Ag and ZnO powders have been used as potent agents with antibacterial and antifungal properties in skin creams and ointments (Pelaz et al., 2017; Pizarro-Cerdá et al., 2012). Furthermore, various studies have demonstrated that smaller NPs sizes have more pronounced toxic effects on bacterial proliferation (Ranjbar and Halaji 2018), although both Ag and ZnO nanoparticles are

effective in inhibiting microorganism growth (Pelaz et al. 2017; Poimenidou et al., 2018).

In the present study, we investigated the antibacterial activity of ZnO:Ag nanoparticles against *L. monocytogenes* strains isolated from cheese. The outcomes revealed that ZnO:Ag NPs were synthesized using a chemical method and SEM, XRD, EDS and FTIR confirmed the successful formation of ZnO:Ag NPs with appropriate shape, size and morphology. Numerous synthesis methods, including physical, chemical and biological approaches, have been employed to create NPs and various studies have indicated that Ag, ZnO and ZnO:Ag NPs can be successfully synthesized using chemical methods (Rolhion and Cossart, 2017). We selected the chemical precipitation method for synthesizing ZnO:Ag NPs due to its advantages, including precise control over stoichiometry, low-temperature processing and chemical homogeneity during synthesis (Seveau 2014).

Based on the results of antibacterial activity and MTT assays, we observed that ZnO:Ag NPs exhibited greater toxicity against *L. monocytogenes* isolates than ZnO NPs alone. The viability of isolates significantly decreased with higher concentrations of both ZnO and ZnO:Ag NPs. Even at lower doses, ZnO:Ag NPs reduced the viability of *L. monocytogenes* isolates, indicating their potential as effective agents against pathogenic bacteria and infectious diseases. Numerous studies have reported the strong antimicrobial activities of nanoparticles against a wide range of bacteria (Singh et al., 2020). Individual studies have also shown that Ag, ZnO and ZnO:Ag NPs possess excellent antibacterial properties and can effectively inhibit the growth of *L. monocytogenes* strains (Sirelkhatim et al., 2015). The MIC and MBC results further demonstrated that *L. monocytogenes* isolates exhibited high sensitivity to lower concentrations of ZnO:Ag compared to ZnO NPs alone.

Both Ag and ZnO are currently being explored as antibacterial and antifungal agents in both microscale and nanoscale formulations. ZnO has demonstrated potent antimicrobial activities, especially when the particle size is reduced. In the case of Ag NPs, they can come into direct contact with bacterial surfaces and/or enter bacterial cells, leading to more effective bactericidal mechanisms (Souza et al., 2019; Sposito et al., 2018). The multifaceted antimicrobial mechanisms of Ag and ZnO NPs are primarily attributed to their small size, high surface-to-volume ratio, and unique physicochemical properties (Sposito et al., 2018). While the exact mechanisms are still under discussion, several hypotheses have been proposed and accepted. Research on ZnO:Ag NPs can further enrich our understanding of nanostructured materials and their mechanisms and phenomena.

Attachment analysis indicated that sub-MIC concentrations of ZnO:Ag NPs reduced both the adhesion and invasion of *L. monocytogenes* isolates to Caco-2 cells. The highest and lowest invasion of Caco-2 cells by *L. monocytogenes* isolates were observed before treatment with ZnO:Ag NPs at 20 hours and after treatment with NPs between six to eight hours. One study previously reported that *L. monocytogenes* isolates treated with TiO2 NPs could reduce internalization in Caco-2 cells. Real-time PCR results revealed that the expression levels of *inlA*, *hlyA* and *prfA* genes were downregulated after the exposure of *L. monocytogenes* to ZnO:Ag NPs, indicating that ZnO:Ag NPs exhibited high antimicrobial and anti-invasion activities.

The mechanism behind the bactericidal effects of Ag NPs is partly understood. The first step involves the accumulation of Ag NPs on the bacterial membrane's surface, followed by their penetration of the cell membrane, which increases cell wall permeability and causes fundamental damage (Abdellrazeq et al., 2014). Zinc oxide nanoparticles (ZnO NPs), one of the most important metallic nanomaterials, have gained increasing attention as antibacterial, anticancer, and antifungal agents in recent years due to their low cost and interesting properties (e.g., conductivity, chemical stability, and safety for humans). It has been demonstrated that the primary antibacterial toxicity mechanisms of ZnO NPs are based on their ability to induce oxidative stress (Venugopal et al., 2017). Ag^{+} ions and Zn^{2+} ions released through the dissolution of ZnO are thought to interact with thiol groups of bacterial respiratory enzymes, leading to increased production of reactive oxygen species (ROS) and progressive oxidative damage, loss of cellular metabolic activity and eventual bacterial cell death (Wang et al., 2017).

L. monocytogenes is a pathogenic bacterium in humans, and its pathogenesis is mediated by virulence factors, including *inlA*, *inlB*, the positive regulatory factor *prfA*, *hlyA* genes and the known listeriolysin O toxin. Listeriolysin O is a major virulence factor of *L. monocytogenes* listeriosis, which is a cholesterol-dependent pore-forming toxin encoded by the *hlyA* gene (Zare et al., 2019). The PrfA protein (encoded by the *prfA* gene) positively regulates *L. monocytogenes* virulence genes, facilitating the transition from an extracellular, flagellum-propelled cell to an intracellular pathogen. Additional bacterial secreted virulence factors include the full-length InlA protein (encoded by the *inlA* gene), which promotes the invasion of enterocytes and the crossing of the intestinal barrier, contributing to the internalization of bacteria into human epithelial cells (Fontecha-Umaña et al., 2020; Gray et al., 2018). Our results demonstrate that ZnO:Ag NPs can reduce the adhesion and invasion of *L. monocytogenes* into cells by downregulating the expression of *L. monocytogenes* virulence genes, such as *inlA, prfA* and *hlyA*.

5. Conclusion

In summary, ZnO and ZnO:Ag NPs were prepared using a precipitation method. The results from XRD, SEM, and FTIR analyses clearly confirm the effective incorporation of ZnO:Ag NPs. ZnO:Ag NPs exhibited better antibacterial activity than ZnO NPs alone against *L. monocytogenes* isolates and Ag-doped ZnO NPs induced larger zones of inhibition in bacterial isolates. The attachment and invasion of all isolates to Caco-2 cells decreased following treatment with sub-MIC concentrations of ZnO:Ag NPs. The analysis of virulence gene transcription levels also revealed that the mRNA levels of *inlA*, *hlyA* and *prfA* genes were downregulated after the exposure of *L. monocytogenes* to sub-MIC concentrations of ZnO:Ag NPs, demonstrating significant anti-invasion and anti-adhesion activity of Ag-doped ZnO NPs against human cell lines. Therefore, ZnO:Ag NPs hold promise for utilization in medicinal and pharmaceutical applications as credible antibacterial, anti-invasion and anti-adhesion agents.

Refereces

Abdellrazeq, G.S., A. M. Kamar and S. M. El-Houshy (2014). "Molecular characterization of Listeria species isolated from frozen fish." Alexandria Journal of Veterinary Sciences 40(1): 1-15.

Ayaz, N. D., B. Onaran, G. Cufaoglu, et al. (2018). "Prevalence and Characterization of Listeria monocytogenes isolated from Beef and Sheep Carcasses in Turkey with Characterization of Locally Isolated Listeriophages as a Control Measure." J Food Prot 81(12): 2045-2053.

Bayda, S., M. Adeel, T. Tuccinardi, et al. (2019). "The History of Nanoscience and Nanotechnology: From Chemical-Physical Applications to Nanomedicine." Molecules 25(1).

Brandt, O., M. Mildner, A. E. Egger, et al. (2012). "Nanoscalic silver possesses broad-spectrum antimicrobial activities and exhibits fewer toxicological side effects than silver sulfadiazine." Nanomedicine 8(4): 478-488.

Burlibaşa, L., M. C. Chifiriuc, M. V. Lungu, et al. (2020). "Synthesis, physico-chemical characterization, antimicrobial activity and toxicological features of AgZnO nanoparticles." Arabian Journal of Chemistry 13(2): 4180-4197.

Cardoza-Contreras, M. N., A. Vásquez-Gallegos, A. Vidal-Limon, et al. (2019). "Photocatalytic and Antimicrobial Properties of Ga Doped and Ag Doped ZnO Nanorods for Water Treatment." Catalysts 9(2): 165.

Carvalho, F., S. Sousa and D. Cabanes (2014). "How Listeria monocytogenes organizes its surface for virulence." Front Cell Infect Microbiol 4: 48.

Dakal, T. C., A. Kumar, R. S. Majumdar, et al. (2016). "Mechanistic Basis of Antimicrobial Actions of Silver Nanoparticles." Front Microbiol 7: 1831.

Dussurget, O., D. Cabanes, P. Dehoux, et al. (2002). "Listeria monocytogenes bile salt hydrolase is a PrfA-regulated virulence factor involved in the intestinal and hepatic phases of

listeriosis." Mol Microbiol 45(4): 1095-1106.

Fahmy, H. M., A. M. Mosleh, A. Abd Elghany, et al. (2019). "Coated silver nanoparticles: Synthesis, cytotoxicity, and optical properties." RSC advances 9(35): 20118-20136.

Fonseca, B. B., P. Silva, A. C. A. Silva, et al. (2019). "Nanocomposite of Ag-Doped ZnO and AgO Nanocrystals as a Preventive Measure to Control Biofilm Formation in Eggshell and Salmonella spp. Entry Into Eggs." Front Microbiol 10: 217.

Fontecha-Umaña, F., A. G. Ríos-Castillo, C. Ripolles-Avila, et al. (2020). "Antimicrobial Activity and Prevention of Bacterial Biofilm Formation of Silver and Zinc Oxide Nanoparticle-Containing Polyester Surfaces at Various Concentrations for Use." Foods 9(4).

Gray, J. A., P. S. Chandry, M. Kaur, et al. (2018). "Novel Biocontrol Methods for Listeria monocytogenes Biofilms in Food Production Facilities." Front Microbiol 9: 605.

Ghosh, T., A. B. Das, B. Jena, et al. (2015). "Antimicrobial effect of silver zinc oxide (Ag-ZnO) nanocomposite particles." Frontiers in Life Science 8(1): 47-54.

Hasan, A., M. Morshed, A. Memic, et al. (2018). "Nanoparticles in tissue engineering: applications, challenges and prospects." Int J Nanomedicine 13: 5637-5655.

Hosu, O., M. Tertis and C. Cristea (2019). "Implication of magnetic nanoparticles in cancer detection, screening and treatment." Magnetochemistry 5(4): 55.

Jamshidi, A. and T. Zeinali (2019). "Significance and Characteristics of Listeria monocytogenes in Poultry Products." Int J Food Sci 2019: 7835253.

Kołodziejczak-Radzimska, A. and T. Jesionowski (2014). "Zinc Oxide-From Synthesis to Application: A Review." Materials (Basel) 7(4): 2833-2881.

Lemon, K. P., N. E. Freitag and R. Kolter (2010). "The virulence regulator PrfA promotes biofilm formation by Listeria monocytogenes." J Bacteriol 192(15): 3969-3976.

Li, C., S. Jin, W. Guan, et al. (2018). "Chemical Precipitation Method for the Synthesis of Nb2O5 Modified Bulk Nickel Catalysts with High Specific Surface Area." J Vis Exp(132).

Miri, A., N. Mahdinejad, O. Ebrahimy, et al. (2019). "Zinc oxide nanoparticles: Biosynthesis, characterization, antifungal and cytotoxic activity." Mater Sci Eng C Mater Biol Appl 104: 109981.

Mirzaei, H. and M. Darroudi (2017). "Zinc oxide nanoparticles: Biological synthesis and biomedical applications." Ceramics International 43(1): 907-914.

Mohammadi, M., A. Maleki, S. Zandi, et al. (2018). "Synthesis and structural properties of Mn-doped ZnO/Graphene nanocomposite." Journal of Advances in Environmental Health Research 6(4): 246-252.

Moulavi, P., H. Noorbazargan, A. Dolatabadi, et al. (2019). "Antibiofilm effect of green engineered silver nanoparticles fabricated from Artemisia scoporia extract on the expression of icaA and icaR genes against multidrug-resistant Staphylococcus aureus." J Basic Microbiol 59(7): 701-712.

Nguyen, B. N. and D. A. Portnoy (2020). "An Inducible Cre-lox System to Analyze the Role of LLO in Listeria monocytogenes Pathogenesis." Toxins (Basel) 12(1).

Jeevanandam, J., A. Barhoum, Y. S. Chan, et al. (2018). "Review on nanoparticles and nanostructured materials: history, sources, toxicity and regulations." Beilstein J Nanotechnol 9: 1050-1074.

Ortega, F. E., M. Rengarajan, N. Chavez, et al. (2017). "Adhesion to the host cell surface is sufficient to mediate Listeria monocytogenes entry into epithelial cells." Mol Biol Cell 28(22): 2945-2957.

Pelaz, B., C. Alexiou, R. A. Alvarez-Puebla, et al. (2017). "Diverse Applications of Nanomedicine." ACS Nano 11(3): 2313-2381.

Pizarro-Cerdá, J., A. Kühbacher and P. Cossart (2012). "Entry of Listeria monocytogenes in mammalian epithelial

cells: an updated view." Cold Spring Harb Perspect Med 2(11).

Ranjbar, R. and M. Halaji (2018). "Epidemiology of Listeria monocytogenes prevalence in foods, animals and human origin from Iran: a systematic review and meta-analysis." BMC Public Health 18(1): 1057.

Poimenidou, S. V., M. Dalmasso, K. Papadimitriou, et al. (2018). "Virulence Gene Sequencing Highlights Similarities and Differences in Sequences in Listeria monocytogenes Serotype 1/2a and 4b Strains of Clinical and Food Origin From 3 Different Geographic Locations." Front Microbiol 9: 1103.

Rolhion, N. and P. Cossart (2017). "How the study of Listeria monocytogenes has led to new concepts in biology." Future Microbiol 12: 621-638.

Seveau, S. (2014). Multifaceted activity of listeriolysin O, the cholesterol-dependent cytolysin of Listeria monocytogenes. MACPF/CDC Proteins-Agents of Defence, Attack and Invasion, Springer: 161-195.

Singh, R., S. Cheng and S. Singh (2020). "Oxidative stress-mediated genotoxic effect of zinc oxide nanoparticles on Deinococcus radiodurans." 3 Biotech 10(2): 66.

Sirelkhatim, A., S. Mahmud, A. Seeni, et al. (2015). "Review on Zinc Oxide Nanoparticles: Antibacterial Activity and Toxicity Mechanism." Nanomicro Lett 7(3): 219-242.

Souza, R. C. d., L. U. Haberbeck, H. G. Riella, et al. (2019). "Antibacterial activity of zinc oxide nanoparticles synthesized by solochemical process." Brazilian Journal of Chemical Engineering 36(2): 885-893.

Sposito, A. J., A. Kurdekar, J. Zhao, et al. (2018). "Application of nanotechnology in biosensors for enhancing pathogen detection." Wiley Interdiscip Rev Nanomed Nanobiotechnol.

Venugopal, K., H. A. Rather, K. Rajagopal, et al. (2017). "Synthesis of silver nanoparticles (Ag NPs) for anticancer activities (MCF 7 breast and A549 lung cell lines) of the crude extract of Syzygium aromaticum." J Photochem Photobiol B 167: 282-289.

Wang, L., C. Hu and L. Shao (2017). "The antimicrobial activity of nanoparticles: present situation and prospects for the future." Int J Nanomedicine 12: 1227-1249.

Zare, M., K. Namratha, S. Alghamdi, et al. (2019). "Novel Green Biomimetic Approach for Synthesis of ZnO-Ag Nanocomposite; Antimicrobial Activity against Food-borne Pathogen, Biocompatibility and Solar Photocatalysis." Sci Rep 9(1): 8303.